JOURNAL OF COMPUTATIONAL PHYSICS 115, 56–64 (1994)

An Exponentially Fitted Finite Volume Method for the Numerical Solution of 2D Unsteady Incompressible Flow Problems

JOHN J. H. MILLER

Department of Mathematics, Trinity College, Dublin 2, Ireland

AND

SONG WANG*

Tritech, 26 Temple Lane, Dublin 2, Ireland

Received August 15, 1991; revised February 15, 1994

In this paper we develop and test an exponentially fitted finite volume method for the numerical solution of the Navier–Stokes equations describing 2D incompressible flows. The method is based on an unstructured Delaunay mesh and its dual Dirichlet tessellation, combined with a locally constant approximation to the flux. This yields a piecewise exponential approximation to the exact solution. Numerical tests are presented for a linear advection–diffusion problem with boundary layers. The method is then applied to the driven cavity problem with Reynolds numbers up to 10^4. The numerical results indicate that the method is robust for a wide range of values of the Reynolds number. In the case $\mathrm{Re} = 10^4$ unsteady solutions are captured if the mesh is sufficiently fine.

1. INTRODUCTION

In this paper we are concerned with the numerical solution of the two-dimensional unsteady incompressible Navier–Stokes equations in the streamfunction–vorticity variables ψ, ω on the domain $\Omega \times (0, T]$ given by

$$\nabla^2\psi - \omega = 0 \tag{1.1}$$

$$\frac{\partial\omega}{\partial t} - \nabla\cdot\left(\frac{1}{\mathrm{Re}}\nabla\omega - \mathbf{a}(\psi)\omega\right) = F \tag{1.2}$$

with the initial and boundary conditions

$$\begin{aligned} &\psi(\mathbf{x}, 0) = \psi_0(\mathbf{x}), \\ &\omega(\mathbf{x}, 0) = \boldsymbol{\omega}_0(\mathbf{x}) \qquad \forall \mathbf{x} \in \Omega \end{aligned} \tag{1.3}$$

$$\psi(\mathbf{x}, t) = \psi_D(\mathbf{x}, t) \qquad \forall (\mathbf{x}, t) \in \partial\Omega \times (0, T] \tag{1.4}$$

$$\nabla\psi(\mathbf{x}, t)\cdot\mathbf{n} = \psi_N(\mathbf{x}, t) \qquad \forall (\mathbf{x}, t) \in \partial\Omega \times (0, T], \tag{1.5}$$

where $\mathrm{Re} > 0$ denotes the Reynolds number, $\mathbf{x} = (x, y)$, $\mathbf{a}(\psi) \equiv \mathbf{curl}\,\psi = (\psi_y, -\psi_x)$, T is a positive constant, $\Omega \in \mathbb{R}^2$ is a bounded open region, $\partial\Omega$ denotes the boundary of Ω, and $\mathbf{n}$ denotes the unit outward normal vector. We remark that there is no physical boundary condition for ω. However, in computations, its nodal values on $\partial\Omega$ can be determined numerically using (1.1), (1.4), and (1.5). We discuss this later in more detail.

It is well known that when Re is large, the solution of (1.1)–(1.5) displays sharp boundary layers so that classical methods may yield erroneous approximate solutions. In attempting to overcome this difficulty upwind schemes are often used. However, it has been pointed out in [2], for example, that these schemes may still give inaccurate solutions. There are also many finite element and finite volume methods for the solution of (1.1)–(1.5). In this paper we discuss the application of an exponentially fitted finite volume method [12, 13], sometimes called the box method, to the solution of (1.1)–(1.5), which has been highly successful in the context of the numerical solution of the semiconductor device equations [3, 13], where $\mathbf{a}$ in (1.2) is irrotational. This method is based on a pair of unstructured dual meshes, known as the Delaunay mesh and its dual Dirichlet tessellation, and on a piecewise constant approximation to the flux proposed independently by Allen and Southwell [1] and by Scharfetter and Gummel [18] which yields a piecewise exponential approximation to the exact solution. The method in higher dimensions has been analysed by some authors for the case where $\mathbf{a}$ in (1.2) is irrotational, for example, [15, 17]. An analysis for the case where $\mathbf{a}$ is not irrotational can be found in [16].

The rest of the paper is organised as follows. In the next section we discuss the finite volume method for a general convection–diffusion equation. The application of the method to (1.1)–(1.2) and the evaluation of the boundary

---

* Present address: School of Mathematics, The University of New South Wales, Sydney 2052, Australia.

0021-9991/94 $6.00

conditions for (1.2) are given in Section 3. In Section 4 we apply this method to a linear advection–diffusion problem with boundary layers. The numerical results show that the rate of convergence in a discrete ε-independent energy norm is $h^{1/2}$ when $\varepsilon \ll h$. We also apply the method to the driven-cavity problem for Reynolds numbers up to 10^4 using both unstructured and structured meshes with mesh sizes $h \approx \frac{1}{60}$. The numerical results show the robustness of this finite volume method. For the case where $\mathrm{Re} = 10^4$ unsteady solutions are obtained.

In what follows we use $|\cdot|$ to denote absolute value, Euclidean length, area or volume, depending on the context.

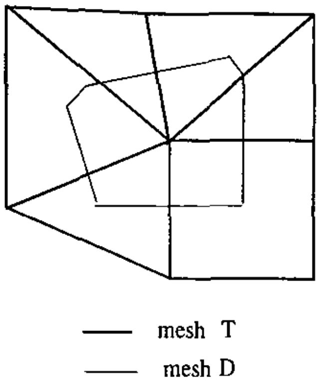

FIG. 2.1. Part of a Delaunay mesh T and dual Dirichlet tessellation D.

2. THE FINITE VOLUME METHOD

In this section we discuss the finite volume method for solving general convection–diffusion equations of the form

$$\partial u/\partial t - \nabla \cdot (\varepsilon \nabla u - \mathbf{a}(\mathbf{x}, t) u) + G(\mathbf{x}, t) u = \mathbf{F}(\mathbf{x}, t) \qquad (2.1)$$

for all $(\mathbf{x}, t) \in \Omega \times (0, T]$ with Dirichlet and Neumann boundary conditions $u(\mathbf{x}, t)|_{\partial\Omega_D} = u_D(\mathbf{x}, t)$ and $\nabla u(\mathbf{x}, t) \cdot \mathbf{n}|_{\partial\Omega_N} = u_N(\mathbf{x}, t)$, where $\mathbf{a}(\mathbf{x}, t) = (a_1(\mathbf{x}, t), a_2(\mathbf{x}, t))$ and ε is a positive constant. It is easy to see that (2.1) contains (1.1) and (1.2) as special cases.

To discuss the finite volume method we first define two partitions of Ω. Let T be any partitioning of $\bar{\Omega}$ by a mixture of triangular and rectangular elements. Let $X = \{\mathbf{x}_i\}_1^{N_X}$ denote the set of all vertices of T and $E = \{e_i\}_1^{N_E}$ the set of all edges of T.

Definition 2.1. T is a Delaunay mesh if, for any element of T, the circumcircle of the element contains no other vertices in X (cf. [4]).

We assume henceforth that T is a Delaunay mesh.

Definition 2.2. The Dirichlet tessellation D corresponding to the Delaunay mesh T is defined by $D = \{d_i\}_1^{N_X}$, where

$$d_i = \{\mathbf{x} \in \Omega : |\mathbf{x} - \mathbf{x}_i| < |\mathbf{x} - \mathbf{x}_j|, \mathbf{x}_j \in X, j \neq i\}$$

for all $\mathbf{x}_i \in X$ (cf. [5]).

We remark that for each $\mathbf{x}_i \in X$, if T is a Delaunay mesh, then d_i is convex and its boundary ∂d_i is the Voronoi polygon [23] obtained by connecting the circumcentres of the elements having $\mathbf{x}_i$ in common. In fact, each segment of ∂d_i is perpendicular to one of the edges joining $\mathbf{x}_i$, and its length equals the distance between the circumcentres of the two elements sharing that edge. Part of a typical Delaunay mesh and its dual Dirichlet tessellation are shown in Fig. 2.1. The Dirichlet tessellation D is a mesh on Ω dual to T and the number of elements in D is equal to N_X. Obviously, T and D are staggered.

We comment that the definition of Delaunay mesh here allows the presence of both triangular and rectangular elements in a mesh. In practice, if four of the mesh nodes form a rectangle we keep them as a rectangular element. This is because whether a rectangle is divided into two triangles or not makes no difference to the discretised equations, as is seen later. In doing so we also remove the non-uniqueness of a standard Delaunay triangulation when four of its nodes form a rectangle.

Without loss of generality, we assume that the edges and the vertices are numbered so that $\{e_i\}_1^M$ is the set of all edges in E that are not on $\partial\Omega_D$ and $\{\mathbf{x}_i\}_1^N$ is the set of all nodes in X that are not on $\partial\Omega_D$.

For each $i = 1, 2, ..., N$, integrating (2.1) over d_i and applying Green's formula to the second term we have

$$\int_{d_i} \frac{\partial u}{\partial t} \, dx \, dy - \int_{\partial d_i} (\varepsilon \nabla u - \mathbf{a} u) \cdot \mathbf{n} \, ds + \int_{d_i} G u \, dx \, dy = \int_{d_i} F \, dx \, dy. \qquad (2.2)$$

For any $t \in (0, T]$ and $i = 1, 2, ..., N$, let $u_i(t)$ be the approximate value of $u(\mathbf{x}, t)$ at $(\mathbf{x}_i, t)$. Using the one-point quadrature rule we have from (2.2)

$$\frac{\partial u_i(t)}{\partial t} |d_i| - \int_{\partial d_i} (\varepsilon \nabla u - \mathbf{a} u) \cdot \mathbf{n} \, ds + G_i(t) \, u_i(t) \, |d_i| = F_i(t) \, |d_i|, \qquad (2.3)$$

where $G_i(t) = G(\mathbf{x}_i, t)$ and $F_i(t) = F(\mathbf{x}_i, t)$. We now consider the approximation of the second term in (2.3).

Let $I_i = \{ j : e_{i,j} \in E\}$ denote the index set of neighbouring nodes of $\mathbf{x}_i$, where $e_{i,j}$ denotes the edge joining $\mathbf{x}_i$ and $\mathbf{x}_j$, as shown in Fig 2.2. Since ∂d_i is polygonal and each of its sides is perpendicular to one of the edges joining $\mathbf{x}_i$, we have

$$\int_{\partial d_i} (\varepsilon \nabla u - \mathbf{a}u) \cdot \mathbf{n}\, ds = \sum_{j \in I_i} \int_{l_{i,j}} (\varepsilon \nabla u - \mathbf{a}u) \cdot \mathbf{e}_{i,j}\, ds, \qquad (2.4)$$

where $l_{i,j}$ denotes the segment of ∂d_i perpendicular to the edge $e_{i,j}$ and is oriented counterclockwise with respect to $\mathbf{x}_i$ (see Fig. 2.2) and $\mathbf{e}_{i,j}$ denotes the unit vector from $\mathbf{x}_i$ to $\mathbf{x}_j$.

For any $t \in (0, T]$, $i = 1, 2, \dots, N$, and $j \in I_i$ we now consider the two-point boundary value problem

$$\begin{aligned} \frac{d}{d\mathbf{e}_{i,j}}\left(\varepsilon \frac{du}{d\mathbf{e}_{i,j}} - a_{i,j}(t)u\right) &= 0 \qquad \text{on } e_{i,j} \\ u(\mathbf{x}_i, t) &= u_i(t), \qquad (2.5) \\ u(\mathbf{x}_j, t) &= u_j(t), \end{aligned}$$

where $a_{i,j}(t)$ is a constant approximation to $\mathbf{a} \cdot \mathbf{e}_{i,j}$ on $e_{i,j}$. Solving this equation analytically we obtain

$$\begin{aligned} f_{i,j}(t) \equiv \varepsilon \frac{du}{d\mathbf{e}_{i,j}} - a_{i,j}u = \frac{\varepsilon}{|e_{i,j}|}\left(B\left(\frac{a_{i,j}(t)\,|e_{i,j}|}{\varepsilon}\right)u_j(t)\right. \\ \left. - B\left(-\frac{a_{i,j}(t)\,|e_{i,j}|}{\varepsilon}\right)u_i(t)\right), \qquad (2.6) \end{aligned}$$

where $B(x)$ is the Bernoulli function defined by

$$B(x) = \begin{cases} \dfrac{x}{e^x - 1} & x \neq 0 \\ 1 & x = 0. \end{cases} \qquad (2.7)$$

Obviously $f_{i,j}(t)$ defines a constant approximation to the integrand on the right side of (2.4). Furthermore, the solution of (2.5) also defines a piecewise exponential approximation to the solution of (2.1) on $e_{i,j}$. Substituting (2.6) into (2.4) and the result into (2.3) we obtain

$$\begin{aligned} &\frac{\partial u_i(t)}{\partial t} + \sum_{j \in I_i} \frac{\varepsilon\,|l_{i,j}|}{|e_{i,j}|\,|d_i|}\left(B\left(-\frac{a_{i,j}(t)\,|e_{i,j}|}{\varepsilon}\right)u_i(t)\right. \\ &\qquad \left. - B\left(\frac{a_{i,j}(t)\,|e_{i,j}|}{\varepsilon}\right)u_j(t)\right) + G_i(t)\,u_i(t) \\ &= F_i(t) \qquad (2.8) \end{aligned}$$

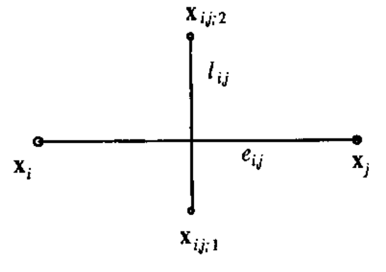

FIG. 2.2. Notation for edges and nodes.

for all $i = 1, 2, \dots, N$. Symbolically we have

$$\left(\mathbf{I}\frac{\partial}{\partial t} + \mathbf{C}(t) + \mathbf{D}(t)\right)\mathbf{u}(t) = \mathbf{F}(t), \qquad (2.9)$$

where $\mathbf{I}$ denotes the unit matrix, $\mathbf{C}(t)$ and $\mathbf{D}(t)$ denote the matrices corresponding respectively to the second and third terms of (2.8), $\mathbf{u}(t) = (u_1(t), \dots, \mathbf{u}_N(t))^{\mathrm{T}}$ and $\mathbf{F}(t) = (F_1(t), \dots, F_N(t))^{\mathrm{T}}$. The matrix $\mathbf{C}(t) = (c_{i,j})$ is unsymmetric unless $a_{i,j}(t) = 0$ for all $i = 1, 2, \dots, N$ and all $j \in I_i$. It is structually symmetric, i.e., if $c_{ij} \neq 0$ then $c_{ji} \neq 0$ and vice versa. However, it is easy to verify that $\mathbf{C}(t)$ is irreducibly diagonally dominant with respect to its columns. Since $c_{ii} > 0$ and $c_{ij} \leqslant 0$ $(i \neq j)$ we have that $\mathbf{C}$ is an M-matrix (cf. [22]). There are several efficient solvers for (2.9), for example, CGS [20] and Bi-CGSTAB [21]. As mentioned in Section 1, analyses of the method for the case that $\mathbf{a}$ is irrotational can be found in, for example, [15, 17]. A complete mathematical analysis of the above method for the case that $\mathbf{a}$ may not be irrotational and that $\partial u/\partial t = 0$ can be found in [16]. There the stability of the method is shown to be independent of ε and the following error estimate for $\varepsilon \ll h$, under some mild conditions on the mesh, is given

$$\|\mathbf{u}_h - \mathbf{u}\|_{1,h} \leqslant \frac{C}{\min_{e_{i,j} \in E} |a_{i,j}|}\, h^{1/2} K(u), \qquad (2.10)$$

where $\mathbf{u}_h = (u_1, u_2, \dots, \mathbf{u}_N)$, $\mathbf{u} = (u(\mathbf{x}_1), u(\mathbf{x}_2), \dots, u(\mathbf{x}_N))$, h is the mesh parameter, C is a positive constant depending only on Ω, $K(u)$ denotes a positive constant depending on the first order seminorms of F, $\mathbf{f} = \varepsilon \nabla u - \mathbf{a}u$ and u, and $\|\cdot\|_h$ is a discrete norm defined by

$$\begin{aligned} \|\mathbf{v}\|_{1,h}^2 = h \sum_{e_{i,j} \in E} \left(\frac{v_j - v_i}{|e_{i,j}|}\right)^2 |e_{i,j}|\,|l_{i,j}| \\ + \sum_{i=1}^{N} v_i^2 \left(\frac{1}{2}\sum_{j \in I_i} a_{i,j}\,|l_{i,j}| + G_i\,|d_i|\right) \qquad (2.11) \end{aligned}$$

for any vector $\mathbf{v} = (v_1, v_2, \dots, v_N)$. The norm defined in (2.11) is a discrete h-dependent energy norm, while the continuous energy norm associated with (2.1) is ε-dependent. The proof of (2.10) is lengthy and we refer to [16]. Since $K(u)$ depends on the first-order seminorms of $\mathbf{f}$ and u, (2.10) does not imply ε-uniform convergence of the method except for some special cases in which $K(u)$ has an ε-independent upper bound.

For (2.10) and (2.11) to apply we need $\frac{1}{2}\sum_{j \in I_i} a_{i,j}\,|l_{i,j}| + G_i\,|d_i| \geqslant 0$ for all i and $\min_{e_{i,j} \in E} |a_{i,j}|$ to be bounded away from 0. The former holds if $\frac{1}{2}\nabla \cdot \mathbf{a} + G \geqslant 0$ (cf. [16]) and the latter is guaranteed if the mesh is chosen such that the angles between all of the $e_{i,j}$ and the characteristic direction $\mathbf{a}$ are locally bounded away from $\pi/2$. We remark that the above method does not need any further restriction on the mesh, such as the condition that it has no obtuse angles. However, in practice, we may need to minimise the maximum angle and maximise the minimum angle so that the method yields more accurate results for a mesh with a fixed number of nodes. This can be achieved by smoothing a given Delaunay triangulation. We also comment that if four mesh nodes form a rectangle, whether the rectangle is divided into two triangles or not, makes no difference to the linear system (2.9). This is because the weights $l_{i,j}$ (cf. Fig. 2.2) associated with the two diagonals are zero, and so these diagonals do not contribute to the linear system.

Finally, for the time discretisation of (2.8) we use the simple backward Euler scheme. Letting $0 = t_0 < t_1 < \cdots < t_k < \cdots < t_K = T$ be a partitioning of $[0, T]$, this leads to

$$\frac{u_i^k - u_i^{k-1}}{t_k - t_{k-1}} + \sum_{j \in I_i} \frac{\varepsilon\, |l_{i,j}|}{|e_{i,j}|\, |d_i|} \left(B\left(-\frac{a_{i,j}^k\, |e_{i,j}|}{\varepsilon} \right) u_i^k - B\left(\frac{a_{i,j}^k\, |e_{i,j}|}{\varepsilon} \right) u_j^k \right) + G_i^k u_i^k = F_i^k \tag{2.10}$$

for all $i = 1, 2, ..., N$ and $k = 1, 2, ..., K$, where the superscript k denotes the nodal values at the kth time level and u_i^k denotes the approximate nodal value of $u_i(t)$ at $t = t_k$. This scheme has first-order accuracy in t and is stable.

3. APPLICATION TO THE STREAMFUNCTION–VORTICITY EQUATIONS

In this section we discuss the application of the exponentially fitted finite volume method developed in the previous section to (1.1) and (1.2). The application to (1.1) is straightforward because it is a linear Poisson equation. The linear system corresponding to (2.12) is

$$\sum_{j \in I_i} \frac{|l_{i,j}|}{|e_{i,j}|\, |d_i|} (\psi_i^k - \psi_j^k) + \omega_i^k = 0 \tag{3.1}$$

for $i = 1, 2, ..., N$ and $k = 1, ..., K$. The boundary condition for (3.1) is taken to be $\psi^k(\mathbf{x}_i) = \psi_D(\mathbf{x}_i)$ for all $\mathbf{x}_i \in \partial\Omega \cap X$.

The application to (1.2) is not straightforward because of the need to evaluate the term $a_{i,j}^k$ in (2.12). Also, since there is no physical boundary condition for (1.2), we need to define a numerical boundary condition for it. We first consider the evaluation of $a_{i,j}$. Let $\mathbf{e} = (e_1, e_2)$ be an arbitrary unit vector. Since $\mathbf{a} = (\psi_y, -\psi_x)$ we have

$$\mathbf{a} \cdot \mathbf{e} = e_1 \frac{\partial \psi}{\partial y} - e_2 \frac{\partial \psi}{\partial x} = \nabla\psi \cdot \mathbf{e}^{\perp},$$

where $\mathbf{e}^{\perp} = (-e_2, e_1)$ denotes the unit vector obtained by rotating $\mathbf{e}$ by 90° counterclockwise. Thus we choose the approximation

$$a_{i,j}^k = \frac{\psi_{i,j;2}^k - \psi_{i,j;1}^k}{|l_{i,j}|} \tag{3.2}$$

where the $\psi_{i,j;k}^k$ $(k = 1, 2)$ denote the computed nodal values at the end-points $\mathbf{x}_{i,j;1}$, $\mathbf{x}_{i,j;2}$ of the edge $l_{i,j}$ of the dual mesh D (cf. Fig. 2.2). Using (3.2) the system of equations corresponding to (2.12) for (1.2) is

$$\frac{\omega_i^k - \omega_i^k}{t_k - t_{k-1}} + \sum_{j \in I_i} \frac{\sigma_{i,j}}{|d_i|} \left(B\left(\frac{\psi_{i,j;1}^k - \psi_{i,j;2}^k}{\sigma_{i,j}} \right) \omega_i^k - B\left(\frac{\psi_{i,j;2}^k - \psi_{i,j;1}^k}{\sigma_{i,j}} \right) \omega_j^k \right) + G_i^k \omega_i^k = F_i^k \tag{3.3}$$

for $i = 1, 2, ..., N$ and $k = 1, 2, ..., K$, where $\sigma_{i,j} = |l_{i,j}|/(\mathrm{Re}\, |e_{i,j}|)$ and $B(x)$ is the Bernoulli function defined in (2.7).

We now consider the boundary condition for (3.3). Let $\mathbf{x}_m \in X \cap \partial\Omega$. Integrating both sides of (1.1) over d_m and using Green's formula we obtain

$$\int_{d_m} \omega(\mathbf{x}_i, t)\, dx\, dy = \int_{\partial d_m} \nabla\psi(\mathbf{x}_i, t) \cdot \mathbf{n}\, ds = \sum_{j \in I_m} \int_{l_{m,j}} \nabla\psi(\mathbf{x}_i, t) \cdot \mathbf{n}\, ds.$$

Noting that ∂d_m consists of edges both inside Ω and on $\partial\Omega$, we make the following approximation at time level k:

$$\omega(\mathbf{x}_m, t_k) \approx \frac{1}{|d_m|} \left[\sum_{j \in I_m, x_j \notin \partial\Omega} (\psi_j^k - \psi(\mathbf{x}_m, t_k)) \frac{|l_{m,j}|}{|e_{m,j}|} + \int_{\partial d_m \cap \partial\Omega} \nabla\psi(\mathbf{x}, t_k) \cdot \mathbf{n}\, ds \right].$$

Finally, using the boundary conditions (1.4) and (1.5) we obtain

$$\omega(\mathbf{x}_m, t_k) \approx \frac{1}{|d_m|} \left[\sum_{j \in I_m, x_j \notin \partial\Omega} (\psi_j^k - \psi_D(\mathbf{x}_m, t_k)) \frac{|l_{m,j}|}{|e_{m,j}|} + \int_{\partial d_m \cap \partial\Omega} \psi_N(\mathbf{x}, t_k)\, ds \right] \tag{3.4}$$

for all $\mathbf{x}_m \in X \cap \partial\Omega$. Obviously (3.4) establishes the relationship between the approximate boundary nodal values of ω and the approximate nodal values of ψ. We remark that when the mesh T is a finite difference mesh, (3.4) reduces to the conventional first-order approximation (see, for example, [11]).

Systems (3.1), (3.3), and (3.4) define a unique approximate solution to (ψ, ω) at the time level k. Obviously these linear systems are coupled. They can be linearised by a Newton-like method or decoupled by a nonlinear Gauss–Seidel method. For details of the latter, we refer to [11, 10].

4. NUMERICAL RESULTS

To test the exponentially fitted finite volume method developed in the previous sections we use it to compute the numerical solution of the following linear advection–diffusion problem, in double precision arithmetic, for a wide range of values of the Reynolds number

$$-\nabla \cdot \left(\frac{1}{\mathrm{Re}} \nabla u - \mathbf{a} u\right) + 2u = F \qquad \text{in} \quad \Omega = (0, 1)^2$$

$$u = 0 \qquad \text{on } \partial\Omega,$$

where $\mathbf{a} = (1, 1)$ and

$$F = x(1 - e^{(x-1)/\varepsilon})[1 + e^{(y-1)/\varepsilon} + y(1 - e^{(y-1)/\varepsilon})] + y(1 - e^{(y-1)/\varepsilon})[1 + e^{(x-1)/\varepsilon} + x(1 - e^{(x-1)/\varepsilon})].$$

Its analytic solution is

$$u_{\text{exact}} = xy(1 - e^{(x-1)/\varepsilon})(1 - e^{(y-1)/\varepsilon}).$$

The solution of this problem has boundary layers along the two sides $\{(1, y) \mid 0 < y < 1\}$ and $\{(x, 1) \mid 0 < x < 1\}$. To solve this problem numerically we start from a Delaunay triangulation with 16 uniformly distributed nodes on $\partial\Omega$ and 9 randomly distributed nodes in Ω. This mesh is then smoothed by recursively moving the interior nodes to the average of their neighbouring nodes. The maximum and minimum angles of the resulting Delaunay triangulation are respectively 106.3° and 32.8° and the mesh parameter $h_1 \approx \frac{1}{4}$. We then refine this mesh repeatedly by adding the mid-points of the edges. Thus we obtain a sequence of meshes corresponding to the mesh parameters $\{h_k\}_1^5$, where $h_k = h_{k-1}/2$ $(k = 2, 3, 4, 5)$. For each $k = 1, 2, 3, 4$ we define a rate of convergence p_k by

$$p_k = \log_2 \frac{\|\mathbf{u}_{h_k} - \mathbf{u}_{\text{exact}}\|_{1,h}}{\|\mathbf{u}_{h_{k+1}} - \mathbf{u}_{\text{exact}}\|_{1,h}},$$

where $\mathbf{u}_{h_k}$ denotes the vector of the nodal values of the approximate solution on the mesh with parameter h_k, $\mathbf{u}_{\text{exact}}$ is the vector of the nodal values of the exact solution and $\|\cdot\|_{1,h}$ is defined in (2.11). Then, we define the computed rate of convergence to be $p = (\sum_{i=1}^{4} p_k)/4$. Based on the above method we also define the computed rates of convergence in the discrete maximum norm

$$\|\mathbf{u}_h - \mathbf{u}_{\text{exact}}\|_{\infty,h} = \max_{1 \leqslant i \leqslant N} |u_i - u_{\text{exact}}(\mathbf{x}_i)|$$

and in the discrete L^2 norm

$$\|\mathbf{u}_h - \mathbf{u}_{\text{exact}}\|_{0,h} = \left(\sum_{i=1}^{N} (u_i - u_{\text{exact}}(\mathbf{x}_i))^2 \, |d_i|\right)^{1/2}.$$

The computed values of p for different values of Re are listed in Table I. From the table we see that when Re is large the computed rate of convergence in the norm $\|\cdot\|_{1,h}$ is about 0.5. This is in agreement with (2.10). The computed rates of convergence p in the norm $\|\cdot\|_{\infty,h}$ and $\|\cdot\|_{0,h}$ are respectively about 0.3 and 0.8. When Re is small the computed rates of convergence in all three norms are close to the classical value 2.

TABLE I

Computed Rates of Convergence in Various Norms for Different Values of Re

Re	$\|\cdot\|_{1,h}$	$\|\cdot\|_{\infty,h}$	$\|\cdot\|_{0,h}$
1	2.00	1.79	1.97
10	1.80	1.58	1.80
100	0.54	0.31	0.90
1000	0.54	0.32	0.78
5000	0.60	0.33	0.78
10000	0.60	0.33	0.78

We now use the exponentially fitted finite volume method to compute the numerical solution of the two-dimensional unsteady incompressible flow problem (1.1)–(1.5) corresponding to the square driven cavity with $\Omega = (0, 1) \times (0, 1)$.

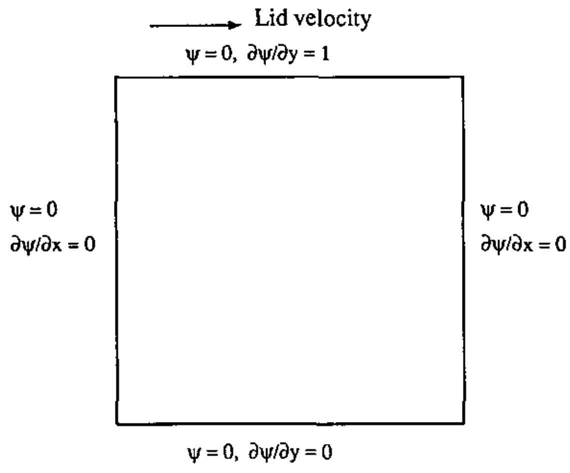

FIG. 4.1. The square driven cavity.

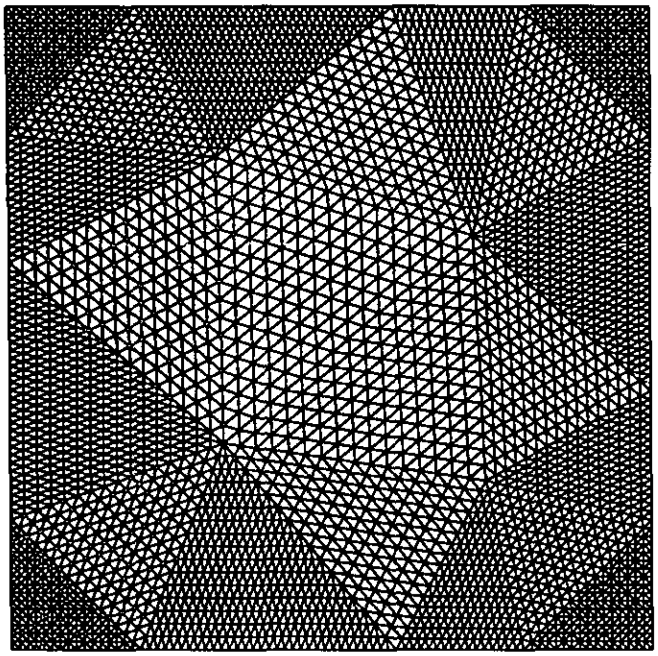

FIG. 4.2. The Delaunay triangulation T_{3489}.

This is depicted in Fig. 4.1. The initial and boundary conditions are

$$\psi_0(\mathbf{x}) = \omega_0(\mathbf{x}) = 0 \qquad \forall \mathbf{x} \in \Omega$$

$$\psi_D(\mathbf{x}, t) = 0 \qquad \forall (\mathbf{x}, t) \in \partial\Omega \times (0, T]$$

$$\psi_N(\mathbf{x}, t) = \begin{cases} 1 & \text{if } y = 1 \\ 0 & \text{otherwise,} \end{cases}$$

where $T > 0$ is chosen to be sufficient large so that the solution is stationary at $t = T$. The size of the time step is chosen to be 0.05. At the kth time step the algebraic systems (3.1), (3.3), and (3.4) are solved iteratively by the Gauss–Seidel method [11], mentioned in the previous section, until the following stopping criterion is satisfied:

$$\|\nabla_h^2 \psi^{k,l} - \omega^{k,l}\|_2 \leqslant 10^{-6},$$

where $\psi^{k,l}$ and $\omega^{k,l}$ denote respectively the vectors of the approximate nodal values of ψ and ω at the lth Gauss–Seidel iteration and the kth time step, ∇_h^2 denotes the discretised Laplace operator appearing in (3.1) and $\|\cdot\|_2$ denotes the Euclidean norm. The stopping criterion for time stepping is chosen to be

$$\max_{x_i \in X} |\omega_i^k - \omega_i^{k-1}| \leqslant 10^{-4}.$$

The decoupled linear system (3.1) is solved by the ICCG method [14], since its coefficient matrix is a symmetric and positive-definite M-matrix. The decoupled linear system (3.4) is solved by the preconditioned CGS method [20].

The problem is first solved on a uniform rectangular mesh $T_{60 \times 60}$ with 3600 mesh nodes and on a triangular mesh T_{3489} with 3489 mesh nodes, as shown in Fig. 4.2. The latter mesh is obtained by first generating a Delaunay triangulation consisting of 16 uniformly distributed boundary nodes and four randomly distributed interior nodes. This triangular mesh is then smoothed recursively by moving each interior node to the average of its neighbouring nodes. Finally the smoothed mesh is refined into a triangular mesh with 3489 mesh nodes by recursively adding a node to the midpoint of each edge. The maximum and minimum angles of the resulting mesh are respectively 108.3° and 26.5°. The

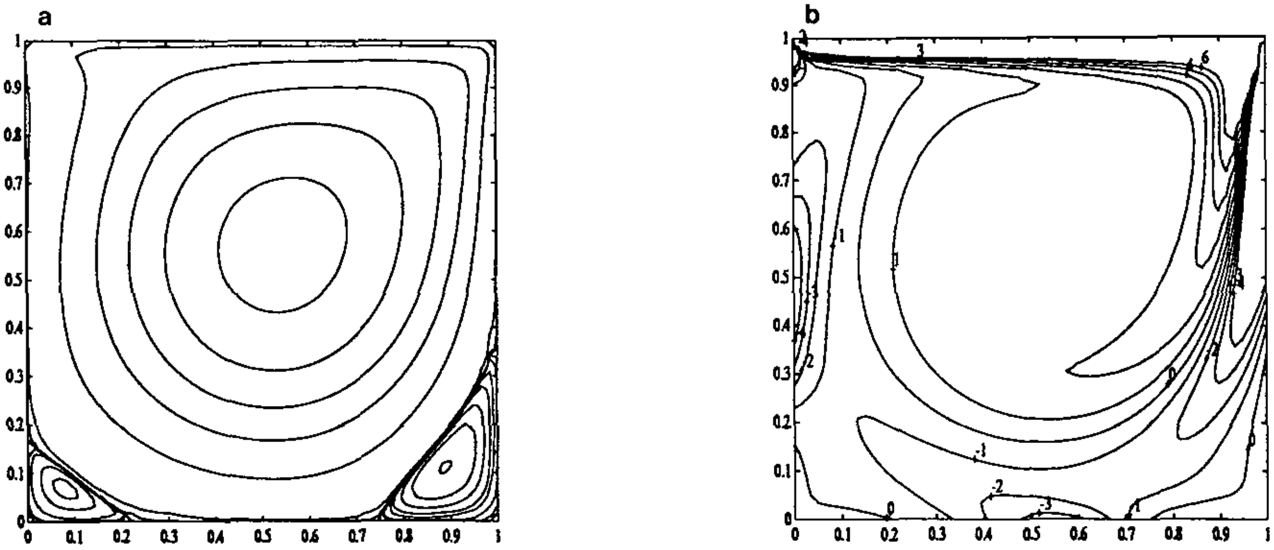

FIG. 4.3. Driven cavity solution for Re = 1000 on $T_{60 \times 60}$: (a) stream function; (b) vorticity.

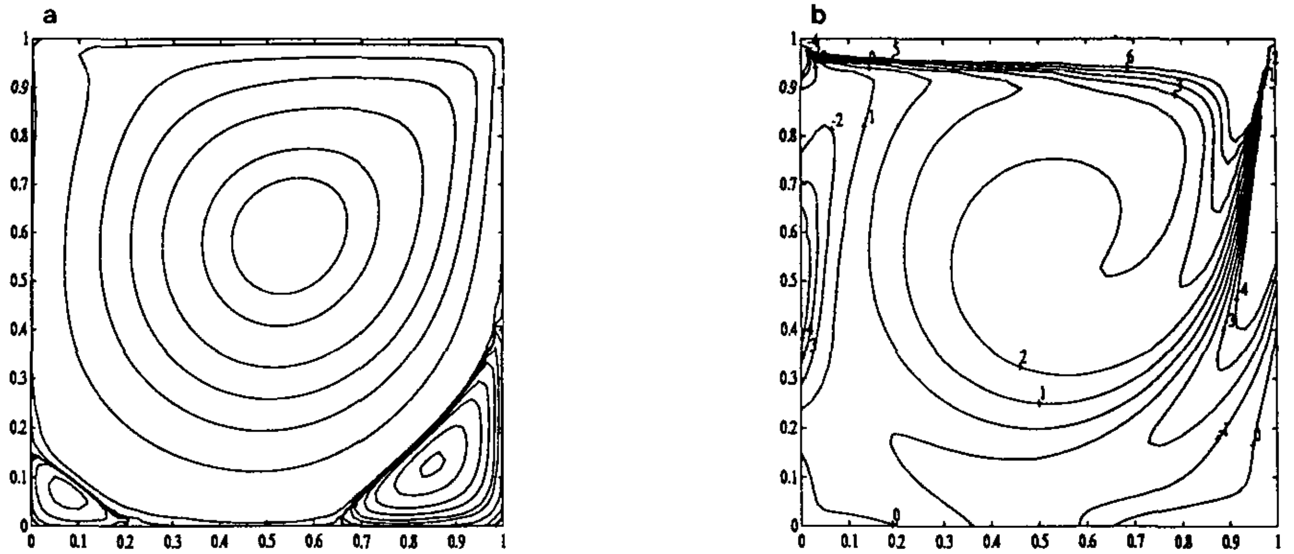

FIG. 4.4. Driven cavity solution for Re = 1000 on T_{3489}: (a) stream function; (b) vorticity.

stream function and vorticity on the two meshes for Re = 1000 are plotted in Fig. 4.3. and Fig. 4.4. These numerical solutions are qualitatively close to those obtained in [6] using a much finer uniform mesh. However, comparing the streamlines in Fig. 4.4 with those in Fig. 4.3, we see that there are small differences in the width and height of the secondary vortices. This may be because on the uniform mesh the numerical method is superconvergent. It seems that the larger the ratio of the maximum and minimum angles, the worse the results. To illustrate this we solve the problem with Re = 1000 on an arbitrary Delaunay triangulation T_{3634} with 3634 mesh nodes. The maximum and minimum angles are then respectively 137.5° and 12.9°. The numerical results are plotted in Fig. 4.5. It is clear that secondary vortices are represented less accurately than by the solution on T_{3489}.

Table II gives the maximum nodal value $|\psi_c|$ of $|\psi|$ and its coordinates (x_c, y_c) for different values of Re obtained on $T_{60\times 60}$, T_{3489}, and on the 257×257 uniform mesh $T_{257\times 257}$ used in [24]. From the table we see that the locations obtained on $T_{60\times 60}$ are more accurate than those from T_{3489}. However, the values of max $|\psi|$ on T_{3489} are closer to those given in [24]. The computed vorticity is extremely sensitive to the discretisation method and mesh, because

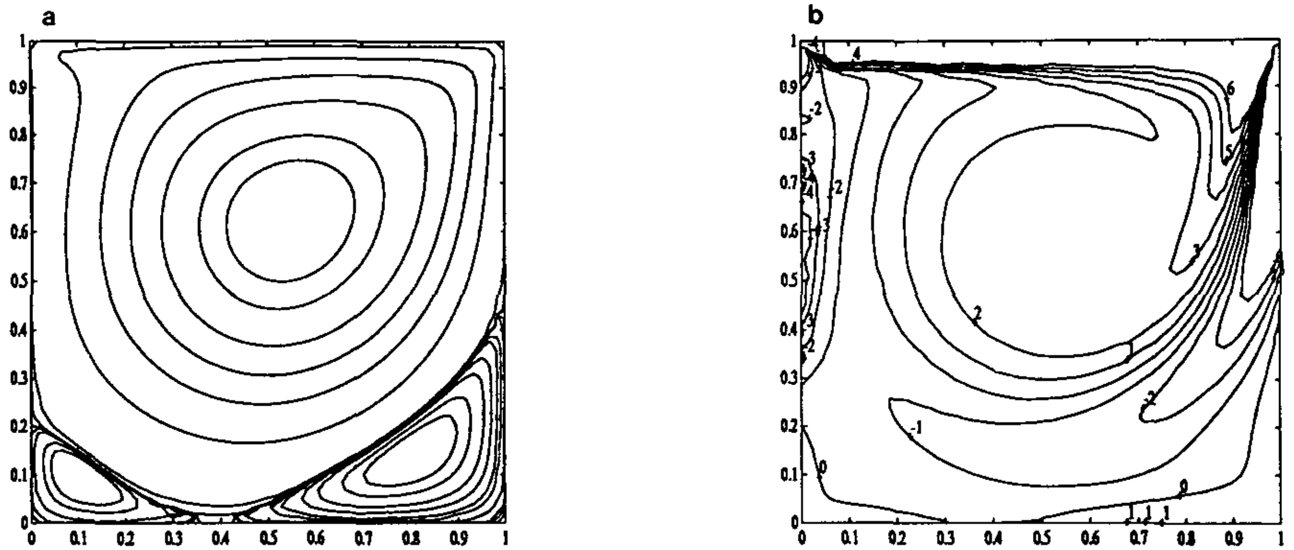

FIG. 4.5. Driven cavity solution for Re = 1000 on T_{3634}: (a) stream function; (b) vorticity.

TABLE II

Maximum Nodal Value of $|\psi|$ and Its Coordinates for Different Reynolds Numbers on Meshes $T_{60\times 60}$, T_{3489}, and $T_{257\times 257}$

	$T_{60\times 60}$		T_{3489}		$T_{257\times 257}$	
Re	x_c, y_c	$\|\psi_c\|$	x_c, y_c	$\|\psi_c\|$	x_c, y_c	$\|\psi_c\|$
100	0.61, 0.75	0.1029	0.63, 0.73	0.1030	0.62, 0.74	0.1035
1000	0.54, 0.58	0.0925	0.55, 0.59	0.1074	0.53, 0.57	0.1193
2000	0.54, 0.58	0.0827	0.55, 0.59	0.1060	0.52, 0.57	0.1217
3200	0.54, 0.56	0.0706	0.55, 0.64	0.1065	0.52, 0.54	0.1234
4000	0.54, 0.54	0.0649	0.57, 0.66	0.1055	0.52, 0.54	0.1234
5000	0.54, 0.54	0.0592	0.57, 0.66	0.1035	0.52, 0.54	0.1240

Note. The results on $T_{257\times 257}$ are taken from [24].

TABLE III

Values of ω at (x_c, y_c) and $(\frac{1}{2}, 1)$ for Different Reynolds Numbers on Meshes $T_{60\times 60}$, T_{3489}, and $T_{257\times 257}$

	$T_{60\times 60}$		T_{3489}		$T_{257\times 257}$	
Re	$\omega(x_c, y_c)$	$\omega(\frac{1}{2}, 1)$	$\omega(x_c, y_c)$	$\omega(\frac{1}{2}, 1)$	$\omega(x_c, y_c)$	$\omega(\frac{1}{2}, 1)$
100	3.14	6.54	3.32	6.59	3.16	6.57
1000	1.74	18.24	2.05	13.57	2.05	14.89
2000	1.38	29.27	2.02	15.16	—	—
3200	1.15	39.63	2.32	14.26	1.99	25.94
4000	1.05	45.12	2.47	13.98	—	—
5000	0.95	50.84	2.59	14.10	1.86	33.01

Note. The results on $T_{257\times 257}$ are taken from [6].

it is singular at the two upper corners and displays sharp boundary layers along the lid of the cavity when Re is large. In Table III we list, without comment, the computed values of vorticity ω_c at the points (x_c, y_c) and $(\frac{1}{2}, 1)$ for different Reynolds numbers using the exponentially fitted method on $T_{60\times 60}$, T_{3489}, and using the upwind method on the uniform mesh $T_{257\times 257}$ (cf. [6]).

Finally the problem is solved for $\mathrm{Re} = 10000$ on T_{3489} and $T_{60\times 60}$. No unsteady solution is found for these two meshes even though it is known that there is no stationary solution for this value of the Reynolds number (cf., for example, [7–9, 19]). However, when the meshes are refined, oscillations in the stream function and vorticity are captured. Figures 4.6 and 4.7 are plots of the minimum nodal value of ψ against time obtained on the 80×80 uniform mesh $T_{80\times 80}$ and on a Delaunay triangulation T_{6561} with 6561 mesh nodes. The maximum and minimum angles of the latter are respectively 110.6° and 31.3°. From the figures we see that in both cases the numerical solution oscillates steadily after a finite time. Note the differences in the scale in the two figures.

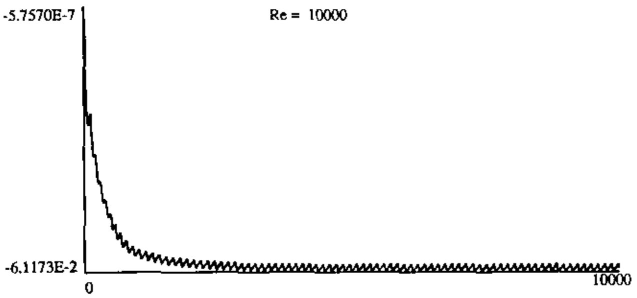

FIG. 4.6. Minimum nodal value of stream function ψ against time step on $T_{80\times 80}$ for the driven cavity problem.

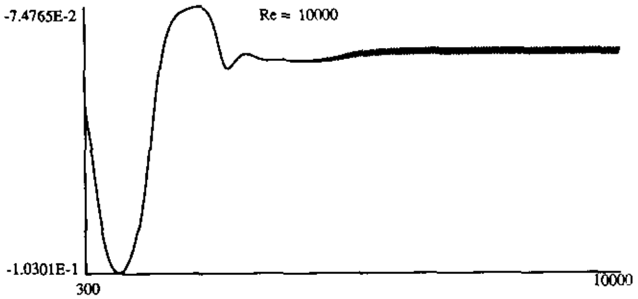

FIG. 4.7. Minimum nodal value of stream function ψ against time step on T_{6561} for the driven cavity problem.

5. CONCLUSION

In this paper we developed and tested an exponentially fitted finite volume method for the numerical solution of the Navier–Stokes equations in the streamfunction–vorticity variables describing 2D incompressible flows. The method is based on an unstructured Delaunay mesh and the corresponding dual Dirichlet tessellation and on a locally constant approximation to the flux, which yields a piecewise exponential approximation to the exact solution. The latter was proposed independently by Allen and Southwell [1] and Scharfetter and Gummel [18]. Numerical tests were presented for a linear advection–diffusion problem and the method was then applied to the driven cavity problem for Reynolds numbers up to 10^4. The numerical results indicated that the method is robust for a wide range of values of the Reynolds number. For the case $\mathrm{Re} = 10^4$ unsteady solutions were captured when the mesh was sufficiently fine.

REFERENCES

1. D. N. de G. Allen and R. V. Southwell, *Quart. J. Mech. Appl. Math.* **8**, 129 (1955).
2. A. Brandt and I. Yavneh, *J. Comput. Phys.* **93**, 128 (1991).
3. E. Buturla, P. Cottrell, B. M. Grossman, and K. A. Salsburg, *IBM J. Res. Develop.* **25** (4), 218 (1981).
4. B. Delaunay, *Izv. Akad. Nauk. SSSR., Math. and Nat. Sci. Div.* **6**, 793 (1934).

5. G. L. Dirichlet, *J. Reine Angew. Math.* **40** (3), 209 (1850).
6. U. Ghia, K. N. Ghia, and C. T. Shin, *J. Comput. Phys.* **48**, 387 (1982).
7. J. W. Goodrich, NASA Technical Memorandum 103141 (unpublished).
8. J. W. Goodrich, K. Gustafson, and K. Halasi, *J. Comput. Phys.* **90** (1),219 (1990).
9. J. W. Goodrich, K. Gustafson, and K. Halasi, *Comput. Phys. Commun.* **65**, 107 (1991).
10. H. K. Gummel, *IEEE Trans. Electron Devices* **ED-11**, 455 (1964).
11. M. M. Gupta and R. P. Manohar, *J. Comput. Phys.* **31**, 265 (1979).
12. R. H. MacNeal, *Quart. Appl. Math.* **11**, (1953).
13. B. J. McCartin, "Discretization of the Semiconductor Device Equations" in *New Problems and New Solutions for Device and Process Modelling*, edited by J. J. H. Miller (Boole Press, Dublin, 1985).
14. J. A. Meijerink and H. A. van der Vorst, *Math. Comput.* **31**, 148 (1977).
15. J. J. H. Miller and S. Wang, *RAIRO Modél. Math. Anal. Numér.* **28**, 123 (1994).
16. J. J. H. Miller and S. Wang, *IMA J. Numer. Anal.* **14**, 257 (1994).
17. M. S. Mock, *COMPEL* **2** (4), 117 (1983).
18. D. L. Scharfetter and H. K. Gummel, *IEEE Trans. Electron. Devices* **ED-16**, 64 (1969).
19. J. Shen, *J. Comput. Phys.* **95**, 228 (1991).
20. P. Sonneveld, *SIAM J. Sci. Statist. Comput.* **10**, 36 (1989).
21. H. A. Van der Vorst, *SIAM J. Sci. Stat. Comput.* **13**, 631 (1992).
22. R. S. Varga, *Matrix Iterative Analysis* (Prentice-Hall, Englewood Cliffs, NJ, (1962).
23. G. Voronoi, *J. Reine Angew. Math.* **134**, 198 (1908).
24. L. B. Zhang, *RAIRO Modél. Math. Anal. Numér.* **24** (1), 133 (1990).